Correlations between supermassive black holes, hot atmospheres, and the total masses of early type galaxies

K. Lakhchaura^{1,2⋆}, N. Truong¹, N. Werner^{1,3,4}

- ¹ MTA-Eötvös University Lendület Hot Universe Research Group, Pázmány Péter sétány 1/A, Budapest, 1117, Hungary
- ²MTA-ELTE Astrophysics Research Group, Pázmány Péter sétány 1/A, Budapest, 1117, Hungary
- ³Department of Theoretical Physics and Astrophysics, Faculty of Science, Masaryk University, Kotlářská 2, Brno, 611 37, Czech Republic
- ⁴School of Science, Hiroshima University, 1-3-1 Kagamiyama, Higashi-Hiroshima 739-8526, Japan

Accepted 2019 July 9. Received 2019 June 17; in original form 2019 April 23.

ABSTRACT

We present a study of relations between the masses of the central supermassive black holes (SMBHs) and the atmospheric gas temperatures and luminosities measured within a range of radii between $R_{\rm e}$ and $5R_{\rm e}$, for a sample of 47 early-type galaxies observed by the *Chandra X-ray Observatory*. We report the discovery of a tight correlation between the atmospheric temperatures of the brightest cluster/group galaxies (BCGs) and their central SMBH masses. Furthermore, our hydrostatic analysis reveals an approximately linear correlation between the total masses of BCGs ($M_{\rm tot}$) and their central SMBH masses ($M_{\rm BH}$). State-of-the-art cosmological simulations show that the SMBH mass could be determined by the binding energy of the halo through radiative feedback during the rapid black hole growth by accretion, while for the most massive galaxies mergers are the chief channel of growth. In the scenario of a simultaneous growth of central SMBHs and their host galaxies through mergers, the observed linear correlation could be a natural consequence of the central limit theorem.

Key words: galaxies: evolution – galaxies: formation – galaxies: active – X-rays: galaxies

1 INTRODUCTION

The masses of central supermassive black holes (SMBHs) are known to correlate with the luminosities and velocity dispersions of the stellar bulge components of their host galaxies, suggesting a coevolution of the two (Magorrian et al. 1998; Gebhardt et al. 2000; Ferrarese & Merritt 2000; Kormendy & Ho 2013; Saglia et al. 2016). Most of the previous studies have explained the observed correlations based on the active galactic nucleus (AGN) feedback induced by the gas accreted onto the SMBH (Silk & Rees 1998; King 2003; Churazov et al. 2005). This picture relies on the assumption that the AGN feedback couples efficiently to the circum-SMBH gas, regulating the growth of both the SMBH and the bulge component.

However, the origin of the observed correlations may also be non-causal (Peng et al. 2007; Jahnke & Macciò 2011; Volonteri et al. 2011). This view is based on the central limit theorem, which suggests that a sufficient number of mergers would lead to the growth of both the mass of the SMBH ($M_{\rm BH}$) and the host galaxy's total mass ($M_{\rm tot}$), resulting in

a linear correlation between the two. As a consequence, any quantity that traces $M_{\rm tot}$, must be a good proxy for $M_{\rm BH}$.

Previous studies (see Ferrarese 2002; Baes et al. 2003) investigated the connection between $M_{\rm BH}$ and $M_{\rm tot}$ (which also includes the mass of the underlying dark matter halo), based on a correlation between the circular velocity ($\nu_{\rm c}$; related to $M_{\rm tot}$) and the stellar velocity dispersion ($\sigma_{\rm e}$; related to $M_{\rm BH}$). This was later rejected based on the argument that it is a result of a 'conspiracy' between baryons and dark matter that also makes the rotation curves flat (Kormendy & Bender 2011). Recently, a relationship was also suggested between the $M_{\rm BH}$ of the brightest cluster/group galaxies (BCGs) and the virial masses of their host clusters/groups, estimated from the temperature of the intra-cluster medium, albeit with a relatively large scatter of \sim 0.4-0.9 dex (see Bogdán et al. 2018; Phipps et al. 2019).

The growth of SMBHs has also been investigated using cosmological simulations. Using the EAGLE simulations, McAlpine et al. (2018) (see also Bower et al. 2017, Fig. 2 & 6) identify three distinct phases of a SMBH's growth depending on the mass of the host galaxy $(M_{\rm gal})$: i) in low-mass galaxies $(M_{\rm gal} << 10^{12}~M_{\odot})$ SMBH's growth is hindered by supernovae driven winds, ii) at $M_{\rm gal} \sim 10^{12}~M_{\odot}$, SMBHs

^{*} lakhchaura.k@gmail.com

undergo a fast growth phase via gas accretion, thanks to the formation of hot atmospheres that efficiently prevent the supernovae-driven winds from buoyantly rising out of the galaxy's central region, and iii) in the largest galaxies $(M_{\rm gal} \gtrsim 10^{12}~M_{\odot})$, SMBHs are massive enough to inject sufficient energy via kinetic mode so that they can regulate the inflow of gas and then retire to a Bondi-like low accretion rate. Weinberger et al. (2018), using the Illustris TNG300 simulations, find a similar pattern of SMBH growth, adding that for the most massive SMBHs $(M_{BH} > 10^{8.5}~M_{\odot})$ mergers become the chief channel of growth (see also Bassini et al. 2019).

In this work, we have investigated the correlation between $M_{\rm BH}$ and the hot galactic atmospheres of the host galaxies, based on the analysis of their *Chandra* X-ray observations¹. The details of the sample are given in §2.1; the data reduction and analysis details are given in §2.2; the results are described in §3 and discussed in §4.

2 SAMPLE AND DATA

2.1 Sample Selection

We have analysed archival Chandra X-ray observations for a sample of early-type galaxies, selected based on the availability of $M_{\rm BH}$ estimates, obtained using stellar/gas dynamics (from Kormendy & Ho 2013, Saglia et al. 2016 and van den Bosch 2016), and archival Chandra X-ray observations. The black hole masses for galaxies undergoing mergers can be severely underestimated (see Kormendy & Ho 2013). Therefore, we excluded the galaxies with recent/ongoing mergers (NGC 1316, NGC 2960, NGC 4382, NGC 5128, IC 1481, NGC 741, NGC 3379). As done in Kormendy & Ho (2013), we also excluded the galaxies with SMBH masses estimated based on kinematics of ionized gas but without the broad emission line widths being taken into account (NGC 2778, NGC 3607, NGC 4261, NGC 4459, NGC 6251, NGC 7052, A1836 BCG, Cygnus A and NGC 4596) as that can also lead to an underestimation of the SMBH mass. We also excluded the well known shell galaxies NGC 3923 and IC 1459. The emission in NGC 821 and NGC 3115 was found to be heavily contaminated by the emission from unresolved point sources and therefore were excluded from the sample. The X-ray spectra extracted for NGC 5845, NGC 4026, NGC 4564 and NGC 7457 had very few counts, and therefore were deemed unusable for the analysis. The SMBH masses for 3C 449 and NGC 3945 were found to be exceedingly uncertain and therefore were excluded from the sample. The properties of the finally selected 47 galaxies, including 18 brightest central cluster/group galaxies (BCGs), 16 non-BCG elliptical galaxies, and 13 lenticular galaxies, are listed in Table 1.

2.2 X-ray Data Reduction and Analysis

The Chandra X-ray observations of all the galaxies were obtained from the High Energy Astrophysics Science Archive Research Centre (HEASARC). We used the Chandra Interactive Analysis of Observations (CIAO) software version 4.9 (Fruscione et al. 2006) and CALDB version 4.7.3 for all the data reduction and spectral extraction. For the spectral analysis, we used the X-ray spectral fitting package XSPEC version 12.9.1 (Arnaud 1996) with ATOMDB version 3.0.7 (Foster et al. 2012). The data were reprocessed using the CIAO tool chandra_repro and time periods with strong background flares were removed using the CIAO script lc_clean. Point sources in the field were detected using the CIAO task wavdetect, verified by visual inspection of the X-ray images and finally removed from all the event files.

The X-ray spectra were extracted from circular regions within the half-light radius ($R_{\rm e}$) i.e. the radius at which the integrated light is half of the total light emitted. For all the galaxies, the $R_{\rm e}$ values were taken from van den Bosch (2016). We also extracted spectra for the central 10 kpc, $3R_{\rm e}$ and $5R_{\rm e}$ regions. For some of the galaxies, the $3R_{\rm e}$ or $5R_{\rm e}$ regions were found to be outside the field of view of the detector. These spectra were not used in the analysis (e.g., NGC 524). For NGC 3842, the deprojected temperature profile shows that the emission in the $3R_{\rm e}$ or $5R_{\rm e}$ regions are mostly dominated by the high temperature cluster plasma and therefore we did not use its spectra from these regions.

For all of the galaxies (except NGC 3842), the standard Chandra blanksky files were used to extract the background spectra. The matching blanksky event files were selected and reprojected to match the source observation coordinates. The time-dependent particle background levels were matched by scaling the blanksky spectra by the 9.5–12 keV count rate ratios of the source and blanksky observations. Due to projection effects, for NGC 3842 (A1367 BCG), the galactic X-ray emission was highly contaminated by the emission from the surrounding high temperature (\sim 4 keV) intracluster medium. Therefore, for NGC 3842, we used the data extracted from an annular region, just outside $R_{\rm e}$, for the background spectrum.

The X-ray spectrum for each galaxy was modeled with an absorbed single-temperature apec component that describes a thermal plasma in collisional ionization equilibrium. The temperature, metallicity, and spectrum normalization were included as free parameters (for details, see Lakhchaura et al. 2018). For the neutral hydrogen column density, we used the Swift Galactic $N_{\rm H}$ tool, which uses the method of Willingale et al. (2013). The redshift was taken from the SIMBAD database (Wenger et al. 2000). An additional thermal bremsstrahlung component with a fixed temperature of 7.3 keV was used to model the unresolved point sources in the field (Irwin et al. 2003). The X-ray temperatures and the 0.5–7.0 keV luminosities for all 47 galaxies in our sample, determined within $R_{\rm e}$, are given in Table 1.

3 RESULTS

The correlations between $M_{\rm BH}$, atmospheric gas temperature (kT), and X-ray luminosity $(L_{\rm X})$ of the galactic atmospheres were determined using the *linmix* package (Kelly

¹ An independent paper submitted for publication by Gaspari et al. (2019) investigates the relation between the masses of supermassive black holes and hot atmospheres based on literature measurements and proposes a different interpretation.

Table 1. The names, distances and effective radii ($R_{\rm e}$, from van den Bosch 2016), hot gas temperatures (kT; within $R_{\rm e}$), 0.5–7.0 keV X-ray luminosities ($L_{\rm X}$; within $R_{\rm e}$), black hole masses ($M_{\rm BH}$), effective stellar velocity dispersions ($\sigma_{\rm e}$), hydrostatic mass estimates ($M_{\rm HE}$; within $5R_{\rm e}$) and references for $M_{\rm BH}/\sigma_{\rm e}$, for the 18 BCGs, 16 non-BCG ellipticals, 13 lenticulars and 2 massive compact relic galaxies, studied in this paper.

Name	Distance (Mpc)	R _e (kpc)	$kT \; (\mathrm{keV})$	$L_{\rm X}~(10^{42}~{\rm erg~s}^{-1})$	$M_{ m BH} \ (10^9 \ M_{\odot})$	$\sigma_{\rm e}~({\rm km~s}^{-1})$	$M_{ m HE}~(5R_{ m e})~(10^{12}~M_{\odot})$	$M_{ m BH}/\sigma_{ m e}$ Ref.
				BCGs				
NGC 315	57.7	10.2	0.70 ± 0.01	0.120 ± 0.035	0.832 ± 0.594	309 ± 29	1.83 ± 0.39	van den Bosch (2016)
NGC 1052	18.1	2.2	0.32 ± 0.02	0.0022 ± 0.0002	0.174 ± 0.116	191±4	0.09 ± 0.02	van den Bosch (2016)
NGC 1332	22.3	4.8	0.62 ± 0.02	0.008 ± 0.004	$1.47^{+0.21}_{-0.20}$	328 ± 9	0.75 ± 0.08	Kormendy & Ho (2013)
NGC 1399	20.9	5.5	1.013 ± 0.004	0.138 ± 0.005	$1.47^{+0.21}_{-0.20} \\ 0.88^{+0.90}_{-0.45} \\ 4.65^{+0.73}_{-0.41}$	315 ± 3	1.49 ± 0.03	Kormendy & Ho (2013)
NGC 1407	28.0	9.3	0.89 ± 0.01	0.093 ± 0.006	$4.65^{+0.73}_{-0.41}$	276 ± 2	1.83 ± 0.06	Kormendy & Ho (2013)
$NGC\ 1550$	51.6	4.6	1.15 ± 0.02	0.551 ± 0.039	$4.65_{-0.41}^{+0.73}$ $3.87_{-0.71}^{+0.61}$	270 ± 10	0.91 ± 0.01	Kormendy & Ho (2013)
NGC 3091	51.2	7.8	0.83 ± 0.01	$0.165 {\pm} 0.023$	$3.87_{-0.71}^{+0.01}$ $3.72_{-0.51}^{+0.11}$	297 ± 12	0.94 ± 0.10	Kormendy & Ho (2013)
NGC 3842	92.2	12.9	1.06 ± 0.03	0.082 ± 0.006	9.10 ± 2.91	270 ± 27	5.15 ± 0.84	Saglia et al. (2016)
$NGC\ 4291$	26.6	2.8	0.49 ± 0.03	0.015 ± 0.006	0.98 ± 0.31	$242 \!\pm\! 12$	0.20 ± 0.02	Kormendy & Ho (2013)
$NGC\ 4486$	16.7	6.6	1.655 ± 0.001	$1.444 {\pm} 0.004$	$6.15^{+0.38}_{-0.37}$	324 ± 20	1.705 ± 0.002	Kormendy & Ho (2013)
$NGC\ 4697$	12.5	4.4	0.33 ± 0.01	0.0015 ± 0.0004	0.20 ± 0.05	177 ± 8	0.21 ± 0.08	Kormendy & Ho (2013)
$NGC\ 5077$	38.7	3.3	0.60 ± 0.05	0.009 ± 0.001	$0.86^{+0.44}_{-0.45}$	222 ± 11	0.63 ± 0.19	Kormendy & Ho (2013)
NGC 5328	64.1	8.7	0.91 ± 0.06	$0.168 {\pm} 0.020$	4.677 ± 1.723	331 ± 15	1.55 ± 0.19	van den Bosch (2016)
NGC 5419	56.2	18.2	1.29 ± 0.03	0.315 ± 0.019	7.24 ± 2.40	367 ± 9	9.00 ± 0.90	Saglia et al. (2016)
NGC 5490	65.2	5.0	0.98 ± 0.05	0.084 ± 0.010	0.537 ± 0.433	257 ± 24	1.16 ± 0.19	van den Bosch (2016)
NGC 5813	32.2	9.1	0.689 ± 0.001	0.496 ± 0.005	0.71 ± 0.09	230 ± 11	1.01 ± 0.01	Saglia et al. (2016)
NGC 5846	24.9	6.3	0.715 ± 0.003	0.172 ± 0.007	1.10 ± 0.15	237±12	0.90 ± 0.01	Saglia et al. (2016)
NGC 7619	51.5	7.4	0.87±0.01	0.124±0.001	$2.30^{+0.15}_{-0.11}$	292±5	1.51±0.05	Kormendy & Ho (2013)
				Non-BCGs				
NGC 541	63.7	8.3	0.72 ± 0.03	0.027 ± 0.009	0.389 ± 0.305	191±4	-	van den Bosch (2016)
$NGC\ 1374$	19.2	1.7	$0.86 {\pm} 0.19$	0.0004 ± 0.0002	$0.59^{+0.06}_{-0.05}$	167 ± 3	_	Kormendy & Ho (2013)
$NGC\ 2892$	86.2	6.8	$0.64 {\pm} 0.09$	0.072 ± 0.014	0.269 ± 0.068	295 ± 20	_	van den Bosch (2016)
NGC 3377	11.0	2.3	0.19 ± 0.03	0.0001 ± 0.00003	0.18 ± 0.09	145 ± 7	_	Kormendy & Ho (2013)
NGC 3608	22.8	3.0	0.33 ± 0.06	0.0013 ± 0.0003	0.47 ± 0.10	182 ± 9	_	Kormendy & Ho (2013)
NGC 3862	84.6	12.0	0.38 ± 0.04	0.037 ± 0.005	0.257 ± 0.219	209 ± 14	_	van den Bosch (2016)
NGC 4374	18.5	3.7	0.73 ± 0.01	0.043 ± 0.003	$0.93_{-0.09}^{+0.10}$ $2.54_{-0.10}^{+0.58}$	296 ± 14	_	Kormendy & Ho (2013)
NGC 4472	17.1	7.8	0.987 ± 0.001	0.311 ± 0.003	$2.54^{+0.58}_{-0.10}$	300 ± 7	_	Kormendy & Ho (2013)
NGC 4473	15.2	2.4	0.38 ± 0.07	0.0005 ± 0.0001	0.09 ± 0.05	190±9	_	Kormendy & Ho (2013)
NGC 4552	15.3	2.8	0.65 ± 0.01	0.0200 ± 0.0002	0.50 ± 0.06	252±12	_	Saglia et al. (2016)
NGC 4621	18.3	3.4	0.23±0.06	0.0003±0.0001	0.40 ± 0.08	225±11	_	Saglia et al. (2016)
NGC 4649	16.5	7.9	0.925 ± 0.002	0.098 ± 0.002	$\begin{array}{c} 4.72 \pm 0.05 \\ 4.72 \pm 1.04 \\ -1.05 \\ 2.44 \pm 0.12 \\ -0.37 \\ 0.27 \pm 0.07 \\ 0.20 \pm 0.08 \end{array}$	380±19	_	Kormendy & Ho (2013)
NGC 4751	26.9	3.3	0.40 ± 0.09	0.011 ± 0.002	$2.44^{+0.12}_{-0.37}$	355 ± 14	_	Kormendy & Ho (2013)
NGC 5576	25.7	4.9	0.31 ± 0.08	0.0009 ± 0.0003	$0.27^{+0.07}_{-0.08}$	183±9	_	Kormendy & Ho (2013)
NGC 7626	38.1	7.4	0.71 ± 0.03	0.039 ± 0.013	0.380 ± 0.289	234 ± 11	_	van den Bosch (2016)
UGC 1841	74.9	30.9	1.31±0.03	0.418±0.058	0.295 ± 0.129	295±27		van den Bosch (2016)
				Lenticulars				
NGC 193	49.7	6.8	0.77 ± 0.03	0.010 ± 0.001	0.251 ± 0.185	187±17	-	van den Bosch (2016)
NGC 383	59.2	12.3	0.93±0.02	0.060 ± 0.013	0.575 ± 0.424	240±17	=	van den Bosch (2016)
NGC 524	24.2	3.6	0.50 ± 0.05	0.011±0.003	$0.87^{+0.09}_{-0.05}$	247±12	=	Kormendy & Ho (2013)
NGC 1023	10.8	3.1	0.32±0.01	0.00056 ± 0.00004	0.042 ± 0.004	205±10	=	Kormendy & Ho (2013)
NGC 3245	21.4	2.5	0.33±0.05	0.0018 ± 0.0004	$0.24_{-0.08}^{+0.03} \\ 0.33_{-0.06}^{+0.15}$	205±10	_	Kormendy & Ho (2013)
NGC 3585	20.5	6.3	0.31 ± 0.02	0.0023 ± 0.0002	$0.33_{-0.06}^{+0.13}$	213±11	_	Kormendy & Ho (2013)
NGC 3665	34.7	6.3	0.40±0.07	0.011 ± 0.002	0.575 ± 0.118	219±10	_	van den Bosch (2016)
NGC 4036	19.0	2.7	0.33 ± 0.05	0.0019 ± 0.0004	0.077 ± 0.064	182±8	_	van den Bosch (2016)
NGC 4203	14.1	2.6	0.29 ± 0.04	0.0011±0.0002	0.066 ± 0.040	129±6	=	van den Bosch (2016)
NGC 4342	22.9	0.6	0.63±0.10	0.0003±0.0001	$0.45^{+0.27}_{-0.15}$	225±11	_	Kormendy & Ho (2013)
NGC 4477	20.8	4.9	0.38 ± 0.01	0.0107 ± 0.0004	0.035 ± 0.024	148±7	_	van den Bosch (2016)
NGC 4526 NGC 6861	16.4 27.3	$\frac{3.5}{2.1}$	0.34 ± 0.02 0.80 ± 0.02	0.0022 ± 0.0002 0.018 ± 0.003	$0.45_{-0.10}^{+0.14} \\ 2.10_{-0.10}^{+0.63}$	222 ± 11 389 ± 3	= =	Kormendy & Ho (2013) Kormendy & Ho (2013)
	27.0	2.1	0.0010.02	Compact Relics	-10.10	00010		22271110114, 66 110 (2010)
M 1 1016	05.0	0.0	0.01 0.00		40177	2041 1750		W. I.I (0017)
Mrk 1216	97.0 56.0	2.3	0.91 ± 0.03 1.02 ± 0.06	0.28 ± 0.09	4.9 ± 1.7	324.1 ± 15.6	_ _	Walsh et al. (2017) Walsh et al. (2016)
NGC 1277	56.9	1.4	1.02±0.00	0.20 ± 0.01	4.9 ± 1.6	250.0 ± 15.3	_	waish et al. (2016)

2007) in *Python* that uses a Bayesian linear regression method that accounts for measurement errors in both axes. The results of the correlation analyses, for the BCGs, non-BCGs, and lenticular galaxies within $R_{\rm e}$, are shown in Fig. 1. For comparison, the figure also shows the correlation of $M_{\rm BH}$ with the effective stellar velocity dispersion ($\sigma_{\rm e}$; taken from Kormendy & Ho 2013 , Saglia et al. 2016 and van den Bosch 2016). The results of similar analyses within the cen-

tral 10 kpc, $3R_e$ and $5R_e$ regions are shown in Figs. A.1, A.2 and A.3, respectively.

From Fig. 1, we see that for the BCGs, $M_{\rm BH}$ correlates strongly with kT within $R_{\rm e}$ ($M_{\rm BH}/{\rm M}_{\odot}=(3.2\pm0.6)\times10^9$ ($kT/{\rm keV})^{2.3\pm0.4}$) with a correlation coefficient of 0.88 ± 0.08 and intrinsic scatter of 0.26 ± 0.08 dex. For the non-BCG elliptical and lenticular galaxies, the correlation is found to be weaker. $M_{\rm BH}$ correlates moderately with the X-ray lumi-

nosity in all sub-classes. In Figs. A.1, A.2 and A.3, we see very similar results also for the central 10 kpc, $3R_{\rm e}$ and $5R_{\rm e}$ regions, respectively. While for the BCGs the $M_{\rm BH}$ -kT correlation is found to be very strong at all radii, for the non-BCG ellipticals and lenticulars, the same correlation is found to be weak at $R_{\rm e}$ and becomes even worse as we move out to larger radii. For the BCGs, $M_{\rm BH}$ correlates better with kT than with $\sigma_{\rm e}$, at all radii. Note that, the observed $M_{\rm BH}$ -kT correlation for the BCGs is also much tighter (scatter $\lesssim 0.28$ dex at all radii) than that with the large scale intracluster medium temperature (scatter ~ 0.4 -0.9 dex; see Bogdán et al. 2018; Phipps et al. 2019).

4 DISCUSSION

The well known $M_{\rm BH}$ - $\sigma_{\rm e}$ correlation reflects the connection between $M_{\rm BH}$ and the stellar mass in the very centre of the galaxy, where the contribution of dark matter to the total mass is negligible. The break-down of the $M_{\rm BH}$ - $\sigma_{\rm e}$ correlation at the high mass end, in BCGs seen in the top right panel of Fig. 1, has been previously discussed (Kormendy & Ho 2013; Hilz et al. 2012) and attributed to post-merger violent relaxation in systems undergoing a large number of mergers.

In hydrostatic equlibrium, kT reflects the total mass $(M_{
m tot})$ of the galaxy and therefore, next to the strong $M_{\rm BH}-kT$ correlation, we also expect a correlation between $M_{\rm BH}$ and $M_{\rm tot}$ for BCGs. We tested this by measuring the hydrostatic masses $(M_{\rm HE})$ of the BCGs within $5R_{\rm e}$, calculated using the relation $M_{\rm HE}(\langle R \rangle) = -(R^2/G\rho_{\rm g}) dP/dr$ at $R = 5R_e$; where G is the gravitational constant. The gas mass density (ρ_g) and the pressure gradient (dP/dr) at R were determined by fitting the deprojected mass density and pressure profiles with powerlaw model fits. As shown in Fig. 2 (left), we find a moderately strong and almost linear (slope of 0.87 ± 0.20) correlation between $M_{\rm BH}$ and $M_{\rm HE}(< 5R_{\rm e})$, with a coefficient of 0.79 ± 0.13 and a scatter of 0.34 ± 0.09 dex. We also calculated the hydrostatic masses within $R_{\rm e}$ and $3R_{\rm e}$ and obtained similar $M_{\rm BH}$ - $M_{\rm HE}$ correlations (see Fig. A.4). The observed scatter could be the result of the inherent uncertainty in the hydrostatic mass measurements due to non-thermal pressure support, which on average contributes $\sim 20-30\%$ of the thermal pressure (Churazov et al. 2010). However, it may also be contributed by additional effects such as abundance gradients, uncertainties in the estimation of $R_{\rm e}$ and other systematic uncertainties (Paggi et al. 2017). At the effective radii of BCGs, dark matter starts to become a significant component of the total mass budget (see Barnabè et al. 2011; Lovell et al. 2018)² and at larger radii of $3R_{\rm e}$ and $5R_{\rm e}$, it becomes the dominant component. The observed moderately strong and almost-linear correlation between $M_{\rm BH}$ and $M_{\rm tot}$, therefore, indicates that for the most massive galaxies in the centres of groups/clusters,

the mass of the central SMBH also correlates with the underlying dark matter halo mass $(M_{\rm DM})$.

We interpret this result in the light of state-of-the-art cosmological simulations. As discussed in the introduction, using results from the TNG300 simulations, Weinberger et al. (2018) found that for the growth of the most massive SMBHs ($M_{\rm BH} > 10^{8.5}~M_{\odot}$), mergers are the most important channel, with the most massive SMBHs ($M_{\rm BH} > 10^{10}~M_{\odot}$) undergoing ~1000 mergers, presumably following the mergers of their host galaxies. Given that the BCGs in our sample are among the most massive galaxies in the Universe, the observed near-linear correlation between the total mass of the galaxy and the central SMBH could be a natural consequence of the non-causal coevolution of SMBHs and galaxies through mergers (Weinberger et al. 2018).

To investigate this further, we divided our sample into "core" and "coreless" galaxies based on the shape of their optical surface-brightness profiles. Using the information available in the literature (Pellegrini 2005; Lauer et al. 2007; Hopkins et al. 2009; Krajnović et al. 2013; Kim & Fabbiano 2015; Saglia et al. 2016; Forbes et al. 2017), we found 25 core and 16 coreless galaxies in our sample (most BCGs and slow-rotating non-BCG ellipticals are core galaxies, while the S0s and other fast rotating ellipticals are typically coreless). The $M_{\rm BH}$ -kT relations for the core and coreless galaxies are shown in Fig. 2 (right). The core galaxies are found to have a very strong $M_{\rm BH}$ -kT correlation (correlation coefficient ~ 0.9 , intrinsic scatter ~ 0.3) while the coreless galaxies are found to have a weak $M_{\rm BH}$ -kT correlation (correlation coefficient ~ 0.5 , intrinsic scatter ~ 0.6). The cores seen in the optical surface-brightness profiles of mostly elliptical galaxies, are believed to have formed by the stellar excavation accompanying the orbital decay of the binary SMBHs that form as a result of dissipationless ("dry") mergers of their host galaxies. The coreless galaxies, on the other hand, are believed to have gone through dissipative ("wet") mergers (Kormendy et al. 2009). The observed tight $M_{\rm BH}$ -kT correlation for the core galaxies could therefore be a natural consequence of the large number of dry galaxy mergers followed by the gradual inspiral and merger of their SMBHs.

The $M_{\rm BH}$ -kT correlation could also be affected by AGN feedback. The $M_{\rm tot}$ -kT correlation for early type galaxies is found to have a much steeper slope than the value expected based on self-similar evolution (\sim 1.5; see Babyk et al. 2018). The relativistic jets emanating from the central AGN in BCGs are likely to increase the temperature with respect to the virial equilibrium value. This effect is expected to be more pronounced in the low-mass galaxies than the high-mass systems (Goulding et al. 2016), which can explain the steepening of the $M_{\rm tot}$ -kT relation (Babyk et al. 2018). While it is non-trivial to assess the exact impact of AGN feedback on the host galaxies, it most likely plays a secondary role in producing the observed $M_{\rm BH}$ -kT correlation.

The low-mass non-BCGs and lenticular galaxies do not show a strong $M_{\rm BH}\text{-}kT$ correlation. This may imply that because of the fewer mergers, the applicability of the central limit theorem is limited and the $M_{\rm BH}\text{-}M_{\rm tot}$ correlation is weaker in these low-mass systems. However, the lack of the $M_{\rm BH}\text{-}kT$ relation does not need to necessarily imply the lack of the $M_{\rm BH}\text{-}M_{\rm tot}$ correlation. In fact, the modest $M_{\rm BH}$ - $L_{\rm X}$ correlation observed for all three classes of galaxies sug-

 $^{^2}$ The observational measurements of DM fraction $(f_{\rm DM})$ within $R_{\rm e}$ are strongly sensitive to the adopted stellar initial mass function (IMF). For example, Barnabè et al. (2011) show that for the most massive early type galaxies $(M_*>10^{10}~M_{\odot})$, similar to our BCGs, adopting the Salpeter IMF results in $f_{\rm DM}~(< R_{\rm e})$ of less than 50% while adopting the Chabrier IMF results in a significantly higher $f_{\rm DM}~(>60\%)$.

Society of the Pacific Conference Series Vol. 101, Astronomical

gests that the $M_{\rm BH}$ - $M_{\rm tot}$ correlation might be in place for all galaxies in our sample. Due to their smaller gravitational potentials, non-BCGs and lenticulars are more sensitive to feedback (Kim & Fabbiano 2013, 2015; Goulding et al. 2016) and for a significant fraction of the lower mass galaxies, the X-ray atmospheres may be in an outflow state (Pellegrini et al. 2018). Ram-pressure stripping of non-BCG galaxies moving through the intra-cluster medium can remove a significant fraction of the galactic atmospheres, altering the thermal state of the gas. These systems, therefore, may not be in hydrostatic equilibrium and their atmospheric temperatures may not accurately reflect the gravitational potential of the host galaxies.

Finally, although mergers and central limit theorem can provide a plausible non-causal explanation for the observed $M_{\rm BH}$ - $kT/M_{\rm BH}$ - $M_{\rm tot}$ correlation, a pure merger picture has a difficulty to account for a class of massive compact 'relic' galaxies. These galaxies observed at $z\sim0$, are likely the remnants of the progenitors of giant ellipticals, which remained largely untouched by mergers since their early, rapid dissipative growth (e.g. Trujillo et al. 2014; Ferré-Mateu et al. 2017; Werner et al. 2018; Buote & Barth 2018, 2019). Fig. 1 shows that the two well-studied massive 'relic' galaxies, NGC 1277 and Mrk 1216, lie on the tight $M_{\rm BH}$ -kT correlation for BCGs. This result is puzzling, because those relic galaxies are believed to have avoided the stage of growth by dry mergers, which suggests that an initial correlation between SMBHs and DM halos could have already existed early in the evolution of these galaxies, following the formation of their X-ray atmospheres. This is consistent with the predictions of the EAGLE simulations, where the rapid growth of black holes following the formation of hot atmospheres (see Bower et al. 2017; McAlpine et al. 2018) results in an $M_{\rm BH}$ which is determined by the binding energy of the halo (see Booth & Schaye 2010, 2011). For BCGs, such an initial correlation could have been subsequently strengthened via numerous gas-free mergers with galaxies hosting central SMBHs. For high-mass galaxies, this scenario implies an $M_{\rm BH}$ - $M_{\rm tot}$ correlation throughout most of the lifetime of the Universe.

5 ACKNOWLEDGEMENT

We are grateful to the referee for the constructive feedback that helped us improve the manuscript significantly. This work was supported by the Lendület LP2016-11 grant awarded by the Hungarian Academy of Sciences. The scientific results reported here are based to a significant degree on data, software and web tools obtained from the High Energy Astrophysics Science Archive Research Center (HEASARC), a service of the Astrophysics Science Division at NASA/GSFC and of the Smithsonian Astrophysical Observatory's High Energy Astrophysics Division. The results are based on observations made by the *Chandra* X-ray Observatory. We thank J. Kormendy, E. Churazov and F. Mernier for useful discussions.

REFERENCES

Arnaud K. A., 1996, in Jacoby G. H., Barnes J., eds, Astronomical

```
Data Analysis Software and Systems V. p. 17
Babyk I. V., McNamara B. R., Nulsen P. E. J., Hogan M. T.,
   Vantyghem A. N., Russell H. R., Pulido F. A., Edge A. C.,
   2018, ApJ, 857, 32
Baes M., Buyle P., Hau G. K. T., Dejonghe H., 2003, MNRAS,
   341, L44
Barnabè M., Czoske O., Koopmans L. V. E., Treu T., Bolton
   A. S., 2011, MNRAS, 415, 2215
Bassini L., et al., 2019, arXiv e-prints, p. arXiv:1903.03142
Bogdán Á., Lovisari L., Volonteri M., Dubois Y., 2018, ApJ, 852,
Booth C. M., Schaye J., 2010, MNRAS, 405, L1
Booth C. M., Schaye J., 2011, MNRAS, 413, 1158
Bower R. G., Schaye J., Frenk C. S., Theuns T., Schaller M.,
   Crain R. A., McAlpine S., 2017, MNRAS, 465, 32
Buote D. A., Barth A. J., 2018, ApJ, 854, 143
Buote D. A., Barth A. J., 2019, arXiv:1902.02938,
Churazov E., Sazonov S., Sunyaev R., Forman W., Jones C.,
   Böhringer H., 2005, MNRAS, 363, L91
Churazov E., et al., 2010, MNRAS, 404, 1165
Ferrarese L., 2002, ApJ, 578, 90
Ferrarese L., Merritt D., 2000, ApJ, 539, L9
Ferré-Mateu A., Trujillo I., Martín-Navarro I., Vazdekis A.,
   Mezcua M., Balcells M., Domínguez L., 2017, MNRAS, 467,
   1929
Forbes D. A., Sinpetru L., Savorgnan G., Romanowsky A. J.,
   Usher C., Brodie J., 2017, MNRAS, 464, 4611
Foster A. R., Ji L., Smith R. K., Brickhouse N. S., 2012, ApJ,
Fruscione A., et al., 2006, in Society of Photo-Optical Instru-
   mentation Engineers (SPIE) Conference Series. p. 62701V,
   doi:10.1117/12.671760
Gaspari M., et al., 2019, arXiv e-prints, p. arXiv:1904.10972
Gebhardt K., et al., 2000, ApJ, 539, L13
Goulding A. D., et al., 2016, ApJ, 826, 167
Hilz M., Naab T., Ostriker J. P., Thomas J., Burkert A., Jesseit
   R., 2012, MNRAS, 425, 3119
Hopkins P. F., Lauer T. R., Cox T. J., Hernquist L., Kormendy
   J., 2009, ApJS, 181, 486
Irwin J. A., Athey A. E., Bregman J. N., 2003, ApJ, 587, 356
Jahnke K., Macciò A. V., 2011, ApJ, 734, 92
Kelly B. C., 2007, ApJ, 665, 1489
Kim D.-W., Fabbiano G., 2013, ApJ, 776, 116
Kim D.-W., Fabbiano G., 2015, ApJ, 812, 127
King A., 2003, ApJ, 596, L27
Kormendy J., Bender R., 2011, Nature, 469, 377
Kormendy J., Ho L. C., 2013, ARA&A, 51, 511
Kormendy J., Fisher D. B., Cornell M. E., Bender R., 2009, ApJS,
Krajnović D., et al., 2013, MNRAS, 433, 2812
Lakhchaura K., et al., 2018, MNRAS, 481, 4472
Lauer T. R., et al., 2007, ApJ, 664, 226
Lovell M. R., et al., 2018, MNRAS, 481, 1950
Magorrian J., et al., 1998, AJ, 115, 2285
McAlpine S., Bower R. G., Rosario D. J., Crain R. A., Schaye J.,
   Theuns T., 2018, MNRAS, 481, 3118
Paggi A., et al., 2017, ApJ, 844, 5
Pellegrini S., 2005, MNRAS, 364, 169
Pellegrini S., Ciotti L., Negri A., Ostriker J. P., 2018, ApJ, 856,
   115
Peng T.-C., Wyrowski F., van der Tak F., Walmsley M., Weiss A.,
   Menten K. M., 2007, in Molecules in Space and Laboratory.
   p. 34
Phipps F., Bogdan A., Lovisari L., Kovacs O. E., Volonteri M.,
   Dubois Y., 2019, arXiv:1903.09965,
```

Saglia R. P., et al., 2016, ApJ, 818, 47

Silk J., Rees M. J., 1998, A&A, 331, L1

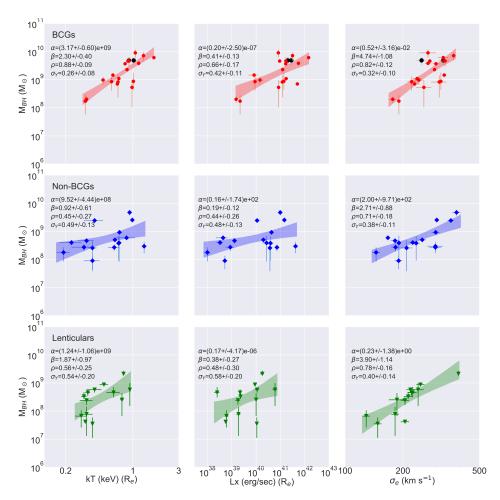


Figure 1. Correlations of the SMBH mass $(M_{\rm BH})$ with the temperature $(kT; {\rm left})$ and 0.5–7.0 keV luminosity $(L_{\rm X}; {\rm centre})$ of the hot gas from within the half light radius $(R_{\rm e})$, and the stellar velocity dispersion $(\sigma_{\rm e}; {\rm right})$ for the BCGs (top row), non-BCG ellipticals (middle row) and lenticulars (bottom row). The intercept (α) , slope (β) , correlation coefficient (ρ) and intrinsic scatter $(\sigma_{\rm Y}; {\rm in \ dex \ units})$, obtained from the log-log correlation analyses $(Y = \alpha X^{\beta})$, and their 68% uncertainties are given in the insets. The shaded areas show the 68% confidence regions for the correlations. The black circles in the top row show the massive compact relic galaxies, Mrk 1216 and NGC 1277.

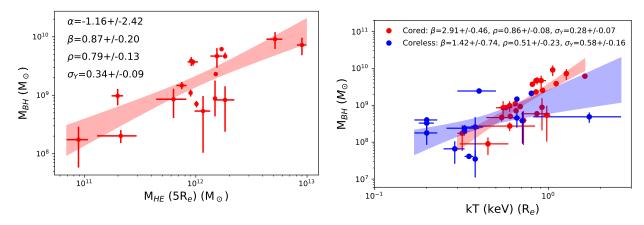


Figure 2. Left: Correlation of the central SMBH mass $(M_{\rm BH})$ with the hydrostatic mass $(M_{\rm HE})$ estimated within $5R_{\rm e}$ for the BCGs. The shaded area shows the 68% confidence region for the correlation. Right: Correlations of the SMBH mass with the hot gas temperature (within $R_{\rm e}$) of the 'cored' (red points) and 'coreless' (blue points) galaxies. The parameters obtained from the correlation analyses are defined in the same way as in Fig. 1, and their 68% uncertainties are given in the insets in both of the panels.

```
Trujillo I., Ferré-Mateu A., Balcells M., Vazdekis A., Sánchez-Blázquez P., 2014, ApJ, 780, L20
Volonteri M., Natarajan P., Gültekin K., 2011, ApJ, 737, 50
Walsh J. L., van den Bosch R. C. E., Gebhardt K., Yıldırım A., Richstone D. O., Gültekin K., Husemann B., 2016, ApJ, 817, 2
Walsh J. L., van den Bosch R. C. E., Gebhardt K., Yıldırım A., Gültekin K., Husemann B., Richstone D. O., 2017, ApJ, 835
Weinberger R., et al., 2018, MNRAS, 479, 4056
Wenger M., et al., 2000, A&AS, 143, 9
Werner N., Lakhchaura K., Canning R. E. A., Gaspari M., Simionescu A., 2018, MNRAS, 477, 3886
Willingale R., Starling R. L. C., Beardmore A. P., Tanvir N. R., O'Brien P. T., 2013, MNRAS, 431, 394
van den Bosch R. C. E., 2016, ApJ, 831, 134
```

APPENDIX A:

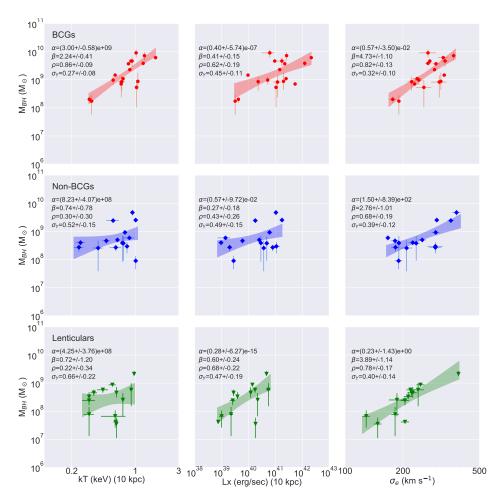


Figure A.1. Same as Fig. 1, but for temperatures and luminosities obtained within r = 10 kpc.

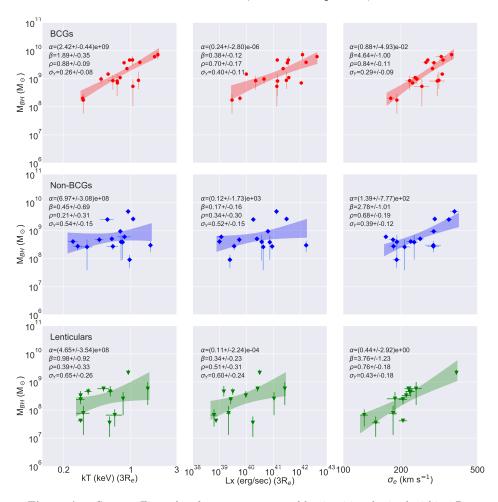


Figure A.2. Same as Fig. 1, but for temperatures and luminosities obtained within $3R_e$.

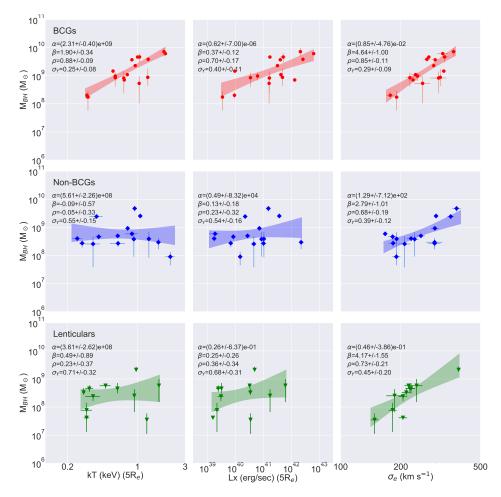


Figure A.3. Same as Fig. 1, but for temperatures and luminosities obtained within $5R_e$.

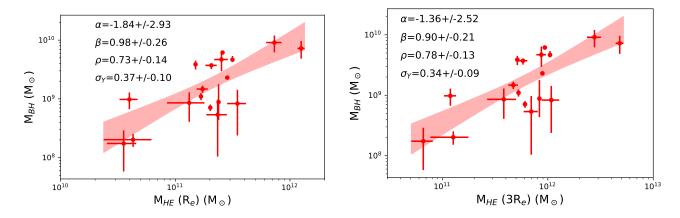


Figure A.4. Same as Fig. 2 (left) but with the hydrostatic masses obtained within $R_{\rm e}$ (left) and $3R_{\rm e}$ (right).